Biosensors and Bioelectronics 133 (2019) 24–31

Contents lists available at ScienceDirect

Biosensors and Bioelectronics

journal homepage: www.elsevier.com/locate/bios

Chemiresistive DNA hybridization sensor with electrospun nanofibers: A method to minimize inter-device variability

Suryasnata Tripathy[a], Vasundhra Bhandari[b], Paresh Sharma[b], Siva Rama Krishna Vanjari[a], Shiv Govind Singh[a,*]

[a] Indian Institute of Technology Hyderabad, 502285, India
[b] National Institute of Animal Biotechnology, Hyderabad 500032, India

ARTICLE INFO

Keywords:
DNA hybridization
Interdigitated electrodes
Chemiresistive
Nanofibers
Electrospinning
Inter-device variability

ABSTRACT

Chemiresistive platforms are best suited for developing DNA hybridization detection systems, owing to their ease of fabrication, simple detection methodology and amenability towards electronics. In this work, we report development of a generic, robust, electrospun nanofiber based interdigitated chemiresistive platform for DNA hybridization detection. The platform comprises of interdigitated metal electrodes decorated with electrospun nanofibers on the top. Two approaches viz., drop casting of graphene doped Mn_2O_3 nanofibers (GMnO) and direct electrospinning of polyaniline/polyethylene oxide (PANi/PEO) composite nanofibers, have been utilized to decorate these electrodes. In both approaches, inter-device variability, a key challenge for converting this proof-of-concept into a tangible prototype/product, has been addressed using a shadow masking technique. Consequently, the relative standard deviation for multiple PANi/PEO nanofiber based chemiresistors has been brought down from 17.82% (without shadow masking) to 4.41% (with shadow masking). The nanofibers are further modified with single-stranded probe DNAs, to capture a desired hybridization event. To establish the generic nature of the platform, detection of multiple target DNAs has been successfully demonstrated. These targets include dengue virus specific consensus primer (DENVCP) and four DNAs corresponding to *Staphylococcus aureus* specific genes, namely *nuc, mecA, vanA* and *protein A*. The chemiresistive detection of DENVCP has been performed in the concentration range of 10 fM – 1 μM, whereas the detection of the other targets has been carried out in the range of 1 pM – 1 μM. Using a 3σ method, we have estimated the limit of detection for the chemiresistive detection of DENVCP to be 1.9 fM.

1. Introduction

DNA hybridization detection is of great medical significance with potential applications in cancerous mutation and viral infection (such as dengue) detection (Boon et al., 2000; Gerry et al., 1999; Kallioniemi et al., 1994; Alwine et al., 1977). Additionally, identification of microbial and viral DNA / RNAs can vastly influence areas such as food adulteration (Abbaspour et al., 2015; Prado et al., 2016), water/soil analysis (Gumpu et al., 2015; Schöler et al., 2017) and disease diagnosis. Keeping these aspects in mind, in this work, we report about a DNA hybridization platform for healthcare and food-analysis applications. Specifically, we target the detection of dengue virus specific consensus primer (DENVCP) and four DNAs corresponding to *Staphylococcus aureus* specific genes. In continuation to our previous work on DENVCP detection (Tripathy et al., 2017a, 2017b), this work is aimed towards developing a point-of-care platform for detecting the viral infection. On the other hand, selection of target DNAs corresponding to *S. aureus* specific genes is largely influenced by our work aimed at milk adulteration detection (Tripathy et al., 2017b). *S. aureus* is a Gram-positive bacterium responsible for numerous mild to chronic infections in humans and animals (Thomer et al., 2016; Mistry et al., 2016), whose presence in raw bovine milk is generally attributed to mastitis, though scarce hygiene is also a major contributor. In Annexure A1 of the supplementary material, different detection schemes for *S. aureus* and related issues have been described briefly. In this study, we aim to detect different *S. aureus* specific genes, namely the species-specific gene, *protein A*, the thermostable nuclease gene *nuc*, along with resistance determinant genes, *mecA* and *vanA*. Note, the proposed platform is no way limited to the above mentioned applications. Instead, the application specific case studies presented in this work are evidence to the generic nature of the platform, which can be used to detect any DNA hybridization of interest.

* Corresponding author.
E-mail address: sgsingh@iith.ac.in (S.G. Singh).

https://doi.org/10.1016/j.bios.2019.03.031
Received 3 January 2019; Received in revised form 2 March 2019; Accepted 17 March 2019
Available online 18 March 2019
0956-5663/

In the past, several sensing approaches have been employed for DNA sensing (Mukhopadhyay et al., 2005; Kim et al., 2004; Yan et al., 2016; Green and Norton, 2015; Peng et al., 2009; Wang and Li, 2011). Among them, the optical and the electrochemical methods have been extensively used towards hybridization detection (Sharon et al., 2010; Ma et al., 2014; Emrani et al., 2016; Drummond et al., 2003; Cui et al., 2015; Akhavan et al., 2012; Huang et al., 2015; Wang et al., 2015). In addition, chemiresistive biosensors have also been adopted for similar applications (Tripathy et al., 2017b; Fu et al., 2017; Bangar et al., 2011; Hahm and Lieber, 2004; Thiha et al., 2018). Such sensors, on account of their simplicity and easy read-out, are tailor-made for low cost point-of-care biosensing, and hence are preferred for the application at hand. Here, by chemiresistors, we mean nanofibers functionalized with application specific capturing agents. Upon interaction with target analytes, the eventual change in the surface charge influences the mobility of charge carriers within the nanofibers, which alters their conductivity (Chandran et al., 2016; Matta et al., 2016; Song and Choi, 2013; Choi et al., 2010). In this context, DNA, being a negatively charged species, proves to be an ideal candidate for chemiresistive biosensing. In such sensors, generally, a single stranded probe DNA is immobilized on to the nanofibers, which then acts as the capturing agent for the corresponding target DNA. Upon hybridization, the conductivity of the probe DNA modified nanofibers gets modulated, in response to a change in surface charge. Keeping this in mind, in this work, we have developed chemiresistive hybridization detection platforms using interdigitated metal electrodes, that are decorated with electrospun nanofiber networks.

Here, we have used electrospinning for synthesizing the nanofibers on account of its simplicity, and the inherent advantages (Bhardwaj and Kundu, 2010; Greiner and Joachim, 2007). In addition to being an efficient way for direct deposition of high aspect ratio (length to diameter) composite nanofibers across metallic electrodes, it further allows one to control the number of nanofibers across the electrodes simply by varying the spinning duration. In this work, we have exploited this simple, yet significant process-advantage, for developing chemiresistors with single and multiple nanofibers. In due process, we address the issue of inter device variability, which is inherent to electrospun nanofibers. It is the resultant of spatial nonuniformity in fiber dimensions, which leads to disparities in their physiochemical and electrical properties (Thompson et al., 2007; Baji et al., 2010; Naraghi et al., 2011). Overcoming this nonuniformity is essential for developing a calibration system that can predict the target analyte concentration with near absolute accuracy, and thereby realizing a tangible prototype/product. Towards this, we have adopted a systematic approach to minimize the variability, and thereby, make the system more consistent. The proposed strategy has been validated using chemiresistors that are fabricated in two distinct approaches, namely (i) direct electrospinning of polymer nanofibers and (ii) drop casting of metal oxide nanofibers. The primary aim, here, is to demonstrate the applicability of the methodology across different platforms, and thereby establish its merit in dealing with the issue of inter-device variability. In subsequent sections, the methodology is outlined in detail.

Herein, towards fabricating the chemiresistive platforms, we have used direct electrospinning of PANi/PEO composite nanofibers, as part of one scheme. The PANi/PEO nanofibers have previously been used to develop DNA biosensors, and are advantageous in terms of their inherent conductivity and ease of surface modification (Tripathy et al., 2017b; Song and Choi, 2013). In the second scheme, for drop casting, we have used GMnO nanofibers. The selection of the same is based on our previous work involving the nanomaterial (Tripathy et al., 2018). We believe, the doped nanomaterial can be used as a chemiresistive transducer on the basis of its improved electrical properties, thanks to graphene doping. We further aim to demonstrate a protocol for using metal-oxide nanofibers as efficient chemi-resistive platforms. Particularly, as the synthesis of such material involves high temperature calcination, which does not favour the use of several substrates (such as plastic, PETs, glass (non-borosilicate)) and non-noble metals (as electrode), direct electrospinning is not a viable option for developing the desired system based on such materials. In this context, the proposed drop casting approach offers an alternative

2. Experimental

2.1. Materials and apparatus

For this work, required chemicals such as polyacrylonitrile (PAN), manganese acetate tetrahydrate, N,N-dimethylformamide (DMF), bovine serum albumin (BSA), human serum albumin (HSA), polyaniline (emeraldine salt) (PANi) and polyethylene oxide (PEO) were purchased from sigma aldrich, USA. Probe and target DNAs corresponding to the dengue virus specific consensus primer, and those specific to the microbial species in milk, were purchased from Bioserve private limited (India). In Annexure A2 of the Supplementary material, the probe and target DNA sequences are listed. In order to facilitate the morphological studies of the electrospun nanofibers, scanning electron microscopy was used in this study. Towards the electrical characterization of the chemiresistive sensors, I-V characteristics were measured using a Keithley 4200 SCS semiconductor parametric analyzer, coupled with a Cascade probestation. A schematic layout of the overall I~V characterization process is presented in Annexure B1 of the Supplementary material.

2.2. Device fabrication

In this work, the chemiresistive platforms were realized using interdigitated microelectrodes developed using standard CMOS fabrication technology. In brief, oxidized Si wafers (P-type) and glass substrates were first subjected to metal deposition (Ti/Au: 20/80 nm) via e-beam evaporation. Subsequently, an optical photolithography process was carried out using a positive photoresist and a printed photomask, for the desired pattern-transfer process. The wafers were then subjected to metal etching for the removal of unwanted metal portions, following which photoresist removal was performed in acetone so as to realize the metal electrodes. A detailed schematic explaining the electrode fabrication process is presented in Fig. 1(a). In addition, in this work, we have also used planar microelectrodes as described in our previous work (Tripathy et al., 2017b).

2.3. Electrospinning of nanofibers

The metal oxide and the polymer nanofibers used in this work were synthesized using the process of electrospinning. Towards the synthesis of graphene doped Mn_2O_3 nanofibers, we used a protocol previously described (Tripathy et al., 2018). In brief, the precursor solution was prepared by adding 20 mg of graphene and 5% (by weight) of manganese acetate tetrahydrate to a PAN/DMF blend (8% by weight) and subjecting the mixture to overnight magnetic stirring. This homogeneous mixture was then electrospun on to a metallic collector using optimal process parameters (flow rate: 30 μL/min, distance: 12 cm, Voltage: 20 kV), and the resulting nanofibers were subsequently calcinated. Post-calcination, the metal oxide nanofibers were collected in powdered form. Following a protocol described before (Tripathy et al., 2017b; Zhang and Rutledge, 2012), we synthesized the PANi/PEO composite conductive nanofibers via electrospinning. The polymer blend (PANI: PEO – 2:1) was prepared in a 3: 1 mixture of chloroform and DMF via magnetic stirring for 24 h. It was subjected to electrospinning at a flow rate of 10 μL/min, with the applied electric field and the spinning-distance being 1.5 kV/cm and 10–12 cm, respectively.

2.4. Protocol for sensor design

For the present study, the chemiresistive biosensors were developed using two separate schemes, as presented in Fig. 1(b). As part of the first

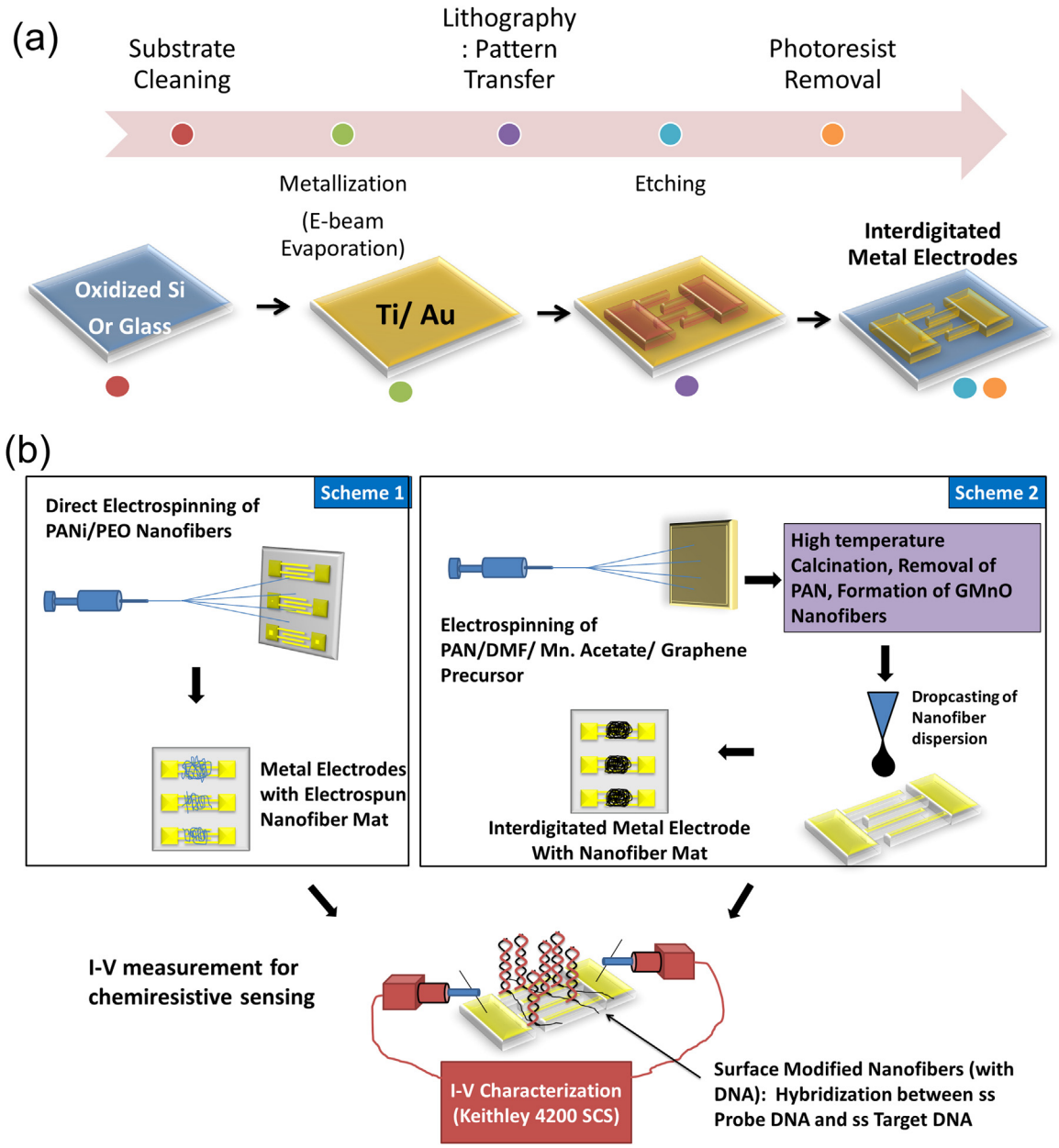

Fig. 1. (a) Schematic representation of the electrode fabrication protocol; (b) Schematic representation of the proposed chemiresistive sensing mechanism. In scheme 1, the chemiresistive platform is developed by direct electrospinning of PANi/PEO Nanofibers on to interdigitated microelectrodes, whereas, in scheme 2, the chemiresistive devices are realized using a drop casting method. The surface modified nanofibers are subjected to I-V measurements for the desired target detection.

scheme, on to a Si/glass substrate with interdigitated metallic electrodes, PANi/PEO nanofibers were directly electrospun, thereby creating conducting pathways between the electrodes. We used a spinning duration of 2 mins for creating devices with multiple nanofibers. Meanwhile, for depositing single PANi/PEO nanofibers, we used planar microelectrodes as described in our previous communication (Tripathy et al., 2017b). Note, in Annexure B2 of the Supplementary material, we have presented a schematic representation of the electrospun nanofibers across the interdigitated electrodes, wherein, we have also provided an approximate resistive circuit model in relation to their I~V characteristics. Post device fabrication, the PANi/PEO nanofibers were surface modified following a protocol described previously (Tripathy et al., 2017b). The surface modified nanofibers were then incubated with 3 µL of probe DNA (1 µM in buffer) at 4 °C for 12 h so as to facilitate the nucleotide immobilization process. In Annexure C of the Supplementary material, we have provided FTIR analysis results confirming successful probe immobilization. Subsequently, the devices were thoroughly rinsed in DI water, and air dried under room temperature. The unoccupied active sites on the nanofibers were blocked with BSA to avoid nonspecific binding of the target DNA.

The second scheme, as presented in Fig. 1(b), deals with the GMnO nanofiber based DNA sensing. Here, the nanofibers were first collected in a powdered form following the protocol described earlier. Subsequently, on to interdigitated metal electrodes, 3 µL of the nanofiber dispersion (in ethanol, 1 mg/mL) was drop casted and the devices were dried at 80 °C for 30 mins so as to facilitate the removal of carrier solvent. This left behind the GMnO nanofibers, forming conducting pathways across the metallic fingers (Refer to Annexure B2 of the Supplementary material for a schematic representation of the nanofibers across the interdigitated electrodes). The thus formed sensing units were then subjected to a previously described surface modification protocol towards the functionalization of the nanofibers (Tripathy

et al., 2018). Subsequently, they were incubated in 3 µL of the buffer solution containing 1 µM of probe DNA (specific to the desired target nucleotide) at 4 °C for 12 h. Post probe DNA immobilization, unspecific binding sites were blocked by BSA.

2.5. Protocols for DNA sensing

In this work, for the target DNA hybridization on to the probe DNA modified biosensor, we have followed a protocol described previously in communications published by our group (Tripathy et al., 2017a, 2018). In brief, on to the probe DNA modified electrodes, 3 µL of target DNA (of different concentrations, in buffer) was drop casted, and the hybridization event was allowed to occur at 37 °C for 1 h. The specific thermal budget was selected based on previously reported literature (Kjallman et al., 2008; Tripathy et al., 2017a, 2018; Zheng and Lin, 2014; Zhang et al., 2018). Also, in our previous communication, we had experimentally optimized the hybridization time needed for the probe-target DNA coupling (Tripathy et al., 2018). Post DNA hybridization, the devices were rinsed carefully so as to remove the non-specifically adsorbed nucleotides, and were air dried. A similar protocol was followed for the selectivity analysis, wherein, the probe DNA modified devices were incubated with non-complementary target DNAs. Towards the stability analysis, probe DNA modified sensors were stored under refrigeration (4 °C) for several days, and subsequently their performance was evaluated. In order to estimate the effect of interference on the proposed chemiresistive sensors, the sensor's response to a particular dose of the target DNA was recorded both in the absence and presence of different interfering species.

3. Result and discussion

3.1. Characterization of electrospun nanofibers

The morphological characterization of the electrospun nanofibers was performed using scanning electron microscopy (SEM). SEM images of the PANi/PEO nanofibers, the uncalcinated and calcinated GMnO nanofibers are shown in Fig. 2(a), (b) and (c) respectively. In terms of diameter, most of the PANi/PEO nanofibers confide to a range of 150–300 nm, while their length extends up to several hundred microns. This accounts for very high aspect ratio, a characteristic feature of electrospun polymer nanofibers. Post calcination, due to the removal of PAN, the GMnO nanofibers show signs of shrinkage. As it turns out, presence of PAN accounts for the smoothness of the nanofibers prior to calcination. Once removed, it leaves behind the composite metal oxide nanofibers, which have uneven surface morphology, and hence, higher effective surface area. As shown in Fig. 2(c), the calcinated nanofibers adhered to a thickness of ~200 nm. Fig. 2(d)-(e) show the electron microscope images of the interdigitated microelectrodes. Here, the finger-width and the inter-finger distance of the metal electrodes are 200 and 80 µm, respectively. Fig. 2(f) shows the planar metal electrodes used in this work. The spatial dimensions of these square shaped electrodes are 200 µm, whereas the inter-electrode distance between two adjacent electrodes is 50 µm. Multiple PANi/PEO nanofibers deposited across microelectrodes, forming resistive pathways, are shown in Fig. 2(g) and (h). As shown, the fibers are oriented unevenly, which induces the inter-device variability in first place. In Fig. 2(i), SEM image of the drop casted nanofiber dispersion is presented. Note, crystallographic, optical and elemental characterization of the GMnO nanofibers have already been reported in great details in our previous communication (Tripathy et al., 2018). Also, the surface modification protocols corresponding to the PANi/PEO and the GMnO nanofibers have previously been validated using Fourier transform infrared spectroscopy (Tripathy et al., 2017b, 2018).

3.2. Electrical characterization of chemiresistors

Electrical characterization of the PANi/PEO nanofibers was performed in the voltage range of −2 V - + 2 V for several devices, with single and multiple nanofibers. Here, the electrical characterization is aimed at estimating the inherent variation in the behaviour of indistinguishable (on the basis of electrode dimensions and electrospinning duration) devices. Specifically, we measured the I~V response of several identical devices, and compared their resistances. Towards ensuring homogeneity among the devices under test, we performed

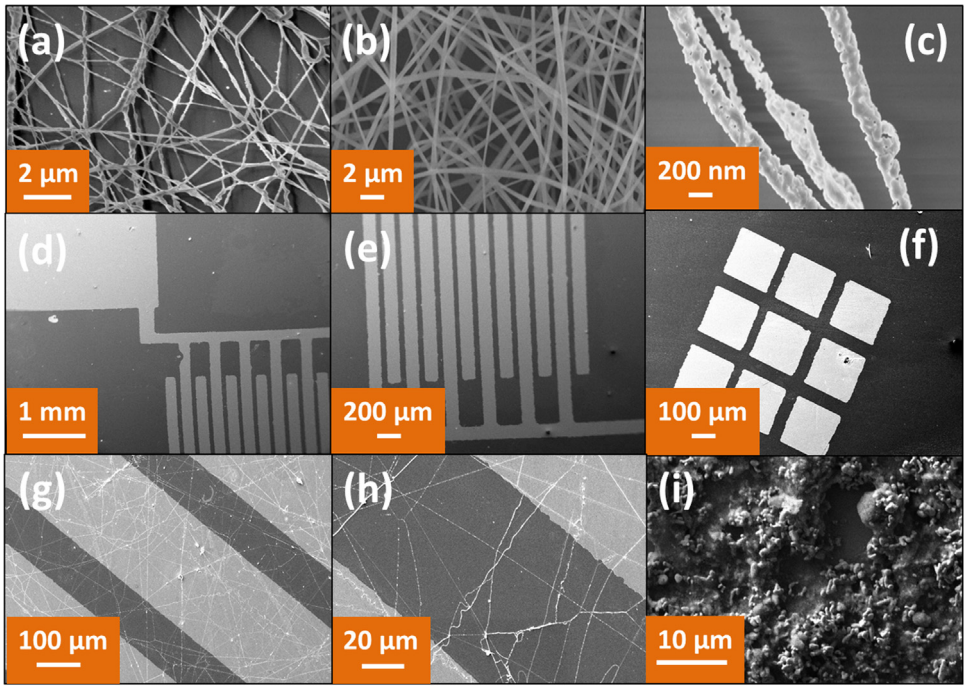

Fig. 2. SEM images of (a) PANi/PEO nanofibers, (b) uncalcinated and (c) calcinated GMnO Nanofibers, (d-e) interdigitated metal electrodes, (f) planar metal electrodes, (g-h) multiple PANi/PEO fibers across metallic fingers and (i) drop casted GMnO nanofiber dispersion.

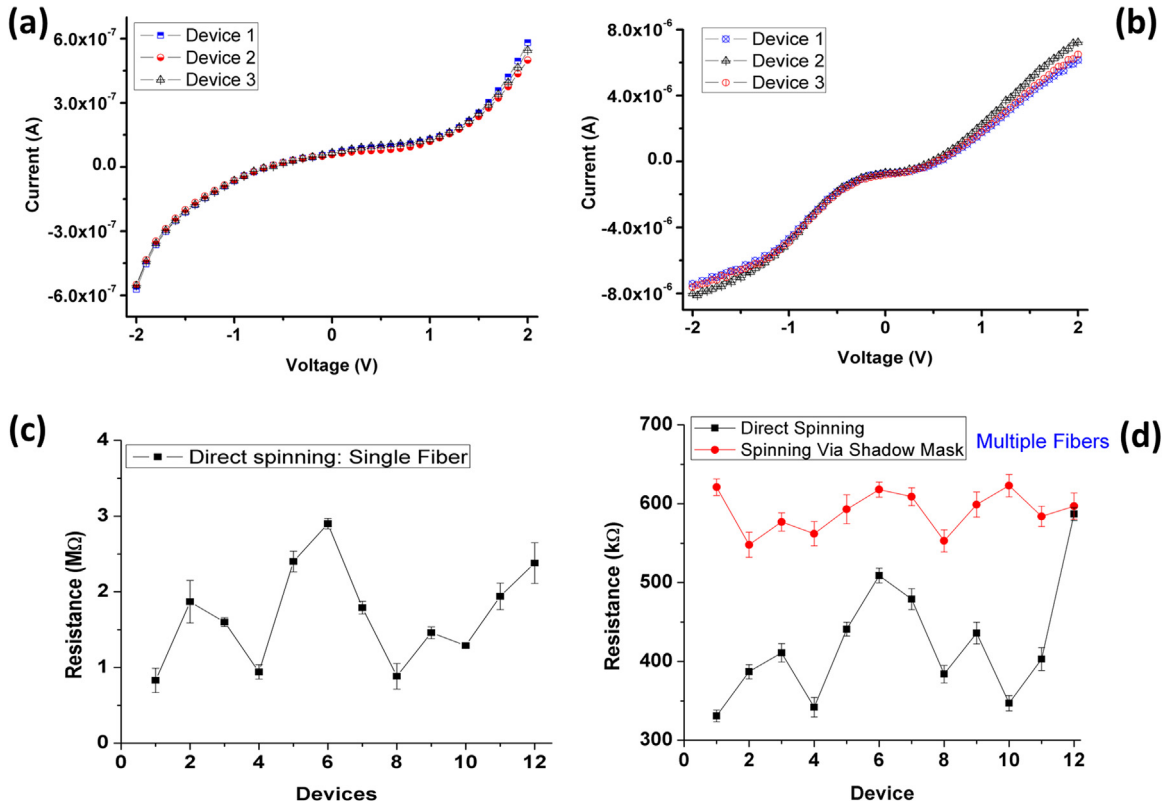

Fig. 3. I∼V characteristics of devices with (a) single and (b) multiple PANi/PEO composite nanofibers; (c) Variation in resistance of devices with single nanofibers deposited by direct electrospinning; (d) Variation in resistance of devices with multiple nanofibers for direct and shadow-mask mediated electrospinning. In Fig (c) and (d), the error bars associated with the data points correspond to the standard deviation values calculated with three successive measurements.

electrospinning for optimal duration on to a single substrate with multiple devices (so as to obtain the desired connectivity), and subsequently used identical devices (carved out of the same substrate) for further characterization. Essentially, the dissimilarity in the device resistance is an indicative of the spatial disparity of electrospun nanofibers connecting them. Fig. 3(a) and (b) show the I∼V response of 3 such identical devices, with single and multiple PANi/PEO nanofibers, respectively. As can be seen, the I∼V response does not approximate an Ohmic behaviour. The current-voltage behaviour for 1D conducting polymers has been shown to follow a power law relationship, which has been attributed to variable range hopping, fluctuation induced tunneling and electric field induced tunneling (Kim et al., 2016; Aleshin et al., 2004). Now, in order to estimate the inter-device variability and the effect of number of nanofibers, we compared the resistance of 12 identical devices, and the comparison is graphically presented in Fig. 3(c) and (d). As shown, for devices having a single nanofiber, the resistance is significantly higher compared to those with multiple nanofibers. This observation is straight forward, as with multiple nanofibers, the overall resistive pathway behaves as a parallel network of several individual resistors (i.e. nanofibers), thereby reducing the effective resistance. However, the relation is not proportional, on account of the fact that the individual resistive pathways are not exactly identical. This non-proportionality is clearly reflected in the resistance values presented in Fig. 3(c) and (d). Here, the following observations can be made in relation to the device characteristics. The resistance of the single nanofibers (Fig. 3(c)) varies significantly across devices (relative standard deviation (RSD), 38.74%), attributing to the spatial variation in the fiber dimensions and their orientation across devices. Such variation is inherent to electrospinning process. In the nano-dimensions, even the slightest change in diameter or length, can lead to drastic changes in the overall device resistance. Also, as seen in Fig. 3(d), even with multiple nanofibers across interdigitated electrodes, such variations in device resistance, though reduced, are not completely eliminated (RSD, 17.82%). This can be attributed to the statistical distribution. Meaning, despite maintaining a uniform spinning duration across devices, the exact number of nanofibers present on an individual device may practically differ with respect to other devices, leading to the statistical disparities. To tackle this, we propose to perform electrospinning through a shadow mask, wherein, during the electrospinning process, only a portion of the interdigitated electrodes is exposed while the rest is covered by the mask. Through this, we intend to ensure that the electrospun nanofibers provide approximately equivalent area-coverage on all the devices, and hence, minimize the inter device variations (in terms of statistical and spatial parameters). As evident from the results shown in Fig. 3(d), with shadow masking, the inter device variation of resistance for PANi/PEO nanofibers has been effectively brought down (RSD, 4.41%), barring a few outliers. This is a demonstration that the proposed strategy can be employed for successful attenuation of inter device variability among electrospun polymer nanofibers.

When modified with the probe DNA, the overall resistance increases in both cases (single and multiple fibers), in response to the negative charge accumulation on surface. Surface charge on conducting nanofibers and nanotubes is belived to modify the electrostatic gate potential, and in turn, change the current-voltage characteristics (Artyukhin et al., 2006; Stafiniak et al., 2011). The resistance values of the probe DNA modified devices are presented in Annexure D of the Supplementary material. As can be inferred, upon probe immobilization, the overall increase in resistance (say, ΔR) is not uniform across devices. Variation in the extent of probe-immobilization across devices can probably induce such an outcome. Further, for multiple nanofiber based devices, ΔR shows relatively less deviation from the mean, as opposed to the single nanofibers. To be exact, the relative standard deviations for the probe modified devices with single and multiple

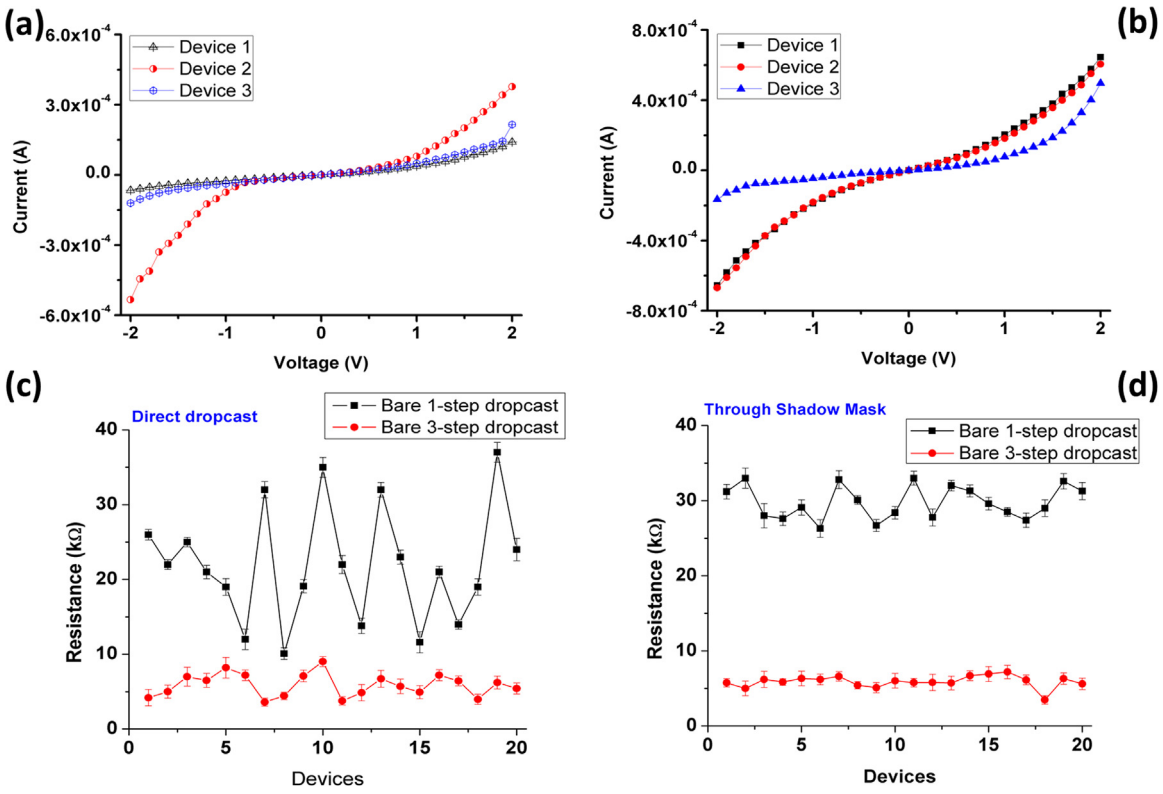

Fig. 4. I~V characteristics of devices with GMnO nanofibers created with (a) 1-step and (b) 3-step drop casting process; Resistance of bare devices where the GMnO nanofiber based chemiresistors are prepared by (c) direct drop cast and (d) shadow-mask mediated drop cast. In both cases, two distinct drop casting protocols (1-step and 3-step) are followed for the device fabrication. In Fig (c) and (d), the error bars associated with the data points correspond to the standard deviation values calculated with three successive measurements.

PANi/PEO nanofibers are 32.6% and 11.3%, respectively. For single nanofibers, due to the spatial variations, and non-uniformity in surface modification, the probe DNA adsorption across devices can vary significantly. However, with multiple nanofibers, as more or less the number of nanofibers, and hence the adsorption sites, are uniform across devices, reduced variations in probe immobilization are expected. Further, when the shadow masking method is used, the RSD for the probe modified devices with multiple nanofibers amounts to 3.26% (see Fig. 2, Annexure D of the Supplementary material). This reduction in the inter-device variability after probe immobilization is significant, as this will enable the development of an accurate calibration system, and thereby ensure precise estimation of the target dose for any blind sample.

Fig. 4 shows the resistance of GMnO nanofiber based chemi-resistors, wherein, the devices are created following two different protocols of drop casting. First, we drop casted 3 μL of the nanofiber dispersion (1 mg/mL) and let dry the devices to remove the carrier solvent (ethanol). The devices were then subjected to I~V measurements (Fig. 4(a) show the I~V response of 3 identical devices) and the corresponding resistance values (averaged over the entire voltage range) were recorded. Here, by identical devices we mean, devices present over a single substrate, having homogeneous device dimensions. For them, when the I~V characteristics are recorded under equal ambience, the variation in the resistance values allows us to estimate the non-uniformity in the drop casting process, and thereby, the inter-device variability. As can be seen in Fig. 4(c), the resistance of the individual devices show severe disparity. Such observations maybe described in line with the imprecisions accompanying the drop casting process. Upon drop casting, the 3 μL droplet spreads differently over different devices, thereby creating fiber networks with assimilar electrical behaviour. To overcome such nonuniformity, in the second approach, we adopted a stepwise drop casting method wherein the 3 μL nanofiber dispersion was drop casted in 3 successive steps (1 μL each). The I~V response corresponding to three such devices is shown in Fig. 4(b). Herein, unlike the first method, the drop casted liquid does not spread over a larger area, thereby limiting the fiber network to an almost identical coverage across devices. In consequence, the variation in device resistance is largely reduced (Fig. 4(c)). To be precise, the standard deviations corresponding to the single step and multistep drop casting protocols stand at 7.72 and 1.52, respectively.

To further reduce the inter-device variability, here also, we adopted a shadow-mask based approach like the previous case, and the corresponding device resistances are shown in Fig. 4(d). In this process, we performed the drop casting (both single step and multistep) via a shadow mask, thereby, exposing equivalent active areas across devices to be decorated by the nanofibers. Eventually, with the shadow masking assisted multi-step drop casting process, the standard deviation for the chemiresistors was brought down to 0.57, indicating reasonable uniformity across devices. This indeed stabilizes the device responses, and allows us to set a relatively uniform baseline for further analysis.

Results presented above are testament to the fact that the proposed methodology for curtailing inter-device variability is applicable to both direct electrospinning as well as drop casting. This provides us with a means to tackle the subtle issue of non-uniformity among electrospun nanofibers. In future, the proposed method may still be optimized to obtain even superior outcome.

3.3. Chemiresistive DNA sensing

Towards the DNA hybridization detection, probe DNA modified devices were exposed to different concentrations of the target DNA for the desired hybridization event to take place. For the target DNAs corresponding to *S. aureus* specific genes, we have used the GMnO nanofiber based chemiresistors, whereas for DENVCP, we have used the

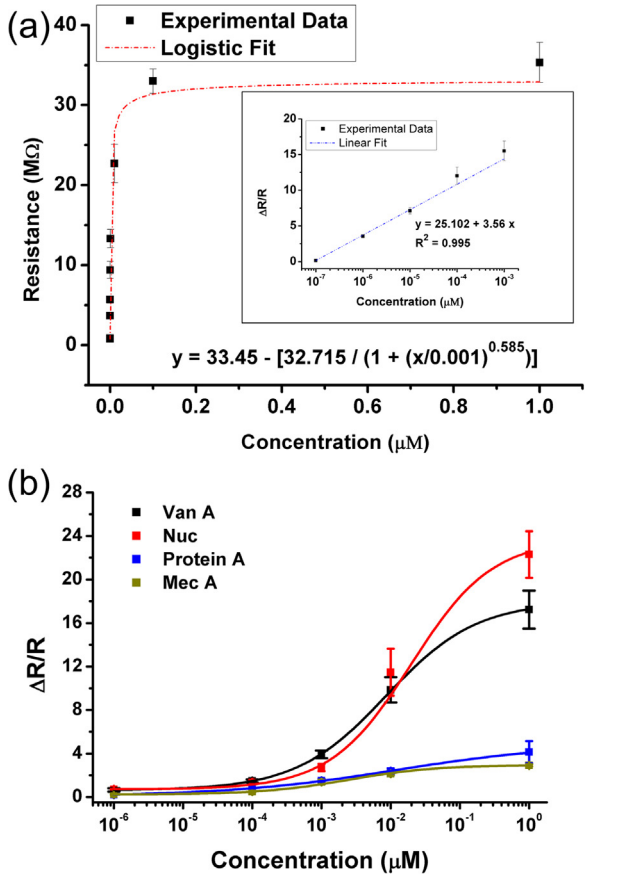

Fig. 5. (a) Calibration curves for DENVCP detection showing the variation of device resistance with the target concentration, along with a 4 parameter logistic fit; Inset: Relation between ΔR/R and the target concentration, with a linear fit. (b) Calibration curves for mecA, vanA, nuc and protein A showing the relation between (ΔR/R) and the target concentration The curve fitting has been done using a four parameter logistics model.

PANi/PEO nanofiber based devices. Post target hybridization, I~V response of the chemiresistors was recorded, and the corresponding resistance values were calculated. The resistance values were compared with the resistance of probe DNA modified devices, and the normalized change in resistance, ΔR/R (where R is the resistance of the device before target hybridization), was derived so as to develop a calibration system.

Fig. 5(a) shows the calibration curve for the DENVCP detection, correlating the average device resistance to the target concentration, in the range of 10 fM – 1 μM. The corresponding I~V responses (for a particular electrode) are presented in Annexure E1 of the Supplementary material. The error values associated with each data point in Fig. 5(a) correspond to the standard deviation obtained using at least four identical bioelectrodes. As can be observed, with the increase in the target concentration, the overall average resistance of the chemiresistors increase. This can be attributed to the increase in surface negative charge upon target hybridization, which influences the charge carrier mobility in the fiber core. The increased device resistance is indeed an indicative of the modified mobility, and hence the target hybridization event. In order to ensure, that the change in device resistance is attributed only to the target hybridization, we have incubated the probe modified nanofibers with blank buffer solutions and recorded the outcome, which shows negligible shift in resistance. The results is provided in Annexure E2 of the Supplementary material. Herein, to derive a calibration equation, we have fitted the experimental data against a four parameter logistics model (Tripathy et al., 2017a, 2018), as given by:

$$y = A2 + \frac{A1-A2}{1 + \left(\frac{x}{x0}\right)^{p}}$$

where, A1 is the maximum asymptote, A2 is the minimum asymptote, x0 is the target concentration corresponding to 50% of the maximum signal change (inflection point) and p is the slope at the inflection point of the sigmoid curve. Additionally, we have calculated the normalized change in device resistance (ΔR/R), and correlated them to corresponding target concentrations. We have performed a linear data fitting for ΔR/R vs. concentration, in the concentration range of 100 fM – 1 nM, and the same is presented in Fig. 5(a) (inset). This linearity does not extend upto the higher target concentrations, where, the relation between ΔR/R and concentration becomes complex and nonlinear. This nonlinearity may be attributed to the complex nature of the system, and the inherent nonuniformity of the hybridization process itself. In order to estimate the theoretical limit of detection for the DENVCP target DNAs, we used the 3σ method (Mahato et al., 2018), where σ is the standard deviation of the blank response. The limiting detection was estimated to be 1.9 fM. Further, we have calculated the sensitivity of the system using standard protocols (Mahato et al., 2018), and the same amounts to 66.05 (MΩ/μM)/cm^2.

Similar experimentation was performed for the four DNA targets corresponding to S. aureus specific genes. Fig. 5(b) below shows the calibration curves for the four DNA targets (range: 1 p.M. – 1 μM), namely nuc, vanA, protein A and mecA, wherein the ΔR/R values are plotted against the respective target concentrations. Here also, we have used the previously described four parameter logistics function to fit the experimental data, and the resulting graphs are appended in Fig. 5(b). The fitting parameters for the four target analytes and the corresponding adj. R^2 values are tabulated in Table 1 in Annexure F of the Supplementary material. Like the previous case, here also we used the 3σ method, for estimating the limiting detection for the four target DNAs. For the reported response, the LoDs for nuc, mecA, vanA and protein A were found to be was estimated to be 0.31 pM, 0.42 pM, 0.67 pM and 0.17 pM, respectively.

We have also analysed the system's efficiency towards DNA hybridization detection in human blood serum (undiluted). Towards this, we have used the DENVCP modified PANi/PEO nanofibers. Here, the target DNA samples were prepared in blood serum, and the hybridization was performed using the protocol described before. The results (see Annexure G of the Supplementary material) refer to the stability of our proposed biosensor platform towards targeted application even in a complex medium like serum. This is a testament of the fact that the platform can be extended for real time DNA sensing, and currently we are working in that direction. Additionally, to evaluate the sensor's performance, we have analysed its stability, selectivity towards noncomplementary targets, and ability to resist interference, following the protocols described in Section 2.5. The experimental results concerning these analyses are presented in Annexure H of the Supplementary material. As inferred, the proposed biosensor platform accounts for reasonably good stability (a mere 1.9% change in the sensor response over a period of 4 weeks), excellent selectivity and tenable interference resistance.

4. Conclusion

In this work, we have reported about the fabrication of chemiresistive biosensing platforms using electrospun nanofibers, and their application in quantitative DNA hybridization detection. Here, using two separate schemes, we have demonstrated two different, yet effective ways, for developing chemiresistive platforms using polymer and metal oxide nanofibers. The devices' ability towards detecting DNA hybridization has been established in this study using five different probe-target nucleotide pairs, which are ultimately aimed at disease diagnosis and food adulteration detection. In relation to a particular target DNA, the proposed biosensing platform has resulted in LoD of

1.9 fM. Further, we have provided ample evidence of the system's stability, selectivity and interference-resistance. Most importantly, we have introduced certain strategic approaches to minimize the inter-device variability, and the same have been validated experimentally. This paves the way for developing biosensor platforms with reduced uncertainty, and therefore, better prediction accuracy.

The future scope of this research is aimed towards developing standalone diagnostic devices with integrated electronics for read-out. Of course, such a system would require an DNA extraction and sample preparation protocol to be performed beforehand, for desired disease diagnosis and genetic studies. However, it is also possible to perform such activities on-chip using microfluidic pathways, and several research has already been published in this direction. Integration of all these platforms on to a single unit is challenging, but it definitely leads towards smarter and improved healthcare.

CRediT authorship contribution statement

Suryasnata Tripathy: Conceptualization, Data curation, Formal analysis, Investigation, Validation, Writing - original draft. **Vasundhra Bhandari:** Methodology, Writing - original draft. **Paresh Sharma:** Methodology, Validation. **Siva Rama Krishna Vanjari:** Supervision, Resources, Writing - review & editing. **Shiv Govind Singh:** Supervision, Resources, Funding acquisition, Writing - review & editing.

Acknowledgment

Parts of the reported work (nanomaterial characterization) were carried out at the Indian Institute of Technology, Bombay under the Indian Nanoelectronics Users program.

Author contributions

The manuscript was written by Suryasnata Tripathy, through contributions from Paresh Sharma and Vasundhara Bhandari. Siva Vanjari and Shiv Govind Singh helped in conceptualization of the work and data interpretation. Suryasnata Tripathy performed the experiments. All authors have given approval to the final version of the manuscript.

Conflict of interest

The authors have no conflict to declare.

Appendix A. Supporting information

Supplementary data associated with this article can be found in the online version at doi:10.1016/j.bios.2019.03.031.

References

Abbaspour, A., Norouz-Sarvestani, F., Noori, A., Soltani, N., 2015. Biosens. Bioelectron. 68, 149–155.
Akhavan, O., Ghaderi, E., Rahighi, R., 2012. ACS Nano 6, 2904–2916.
Aleshin, A.N., Lee, H.J., Park, Y.W., Akagi, K., 2004. Phys. Rev. Lett. 93, 196601.
Alwine, J.C., Kemp, D.J., Stark, G.R., 1977. Proc. Natl. Acad. Sci. USA 74, 5350–5354.
Artyukhin, A.B., Stadermann, M., Friddle, R.W., Stroeve, P., Bakajin, O., Noy, A., 2006. Nano Lett. 6, 2080–2085.
Baji, A., Mai, Y.W., Wong, S.C., Abtahi, M., Chen, P., 2010. Compos. Sci. Technol. 70, 703–718.
Bangar, M.A., Shirale, D.J., Purohit, H.J., Chen, W., Myung, N.V., Mulchandani, A., 2011. Electroanalysis 23, 371–379.
Bhardwaj, N., Kundu, S.C., 2010. Biotechnol. Adv. 28, 325–347.
Boon, E.M., Ceres, D.M., Drummond, T.G., Hill, M.G., Barton, J.K., 2000. Nat. Biotechnol. 18, 1096.
Chandran, G.T., Li, X., Ogata, A., Penner, R.M., 2016. Anal. Chem. 89, 249–275.
Choi, J., Lee, J., Choi, J., Jung, D., Shim, S.E., 2010. Synth. Met. 160, 1415–1421.
Cui, H.F., et al., 2015. Anal. Chem. 87, 1358–1365.
Drummond, T.G., Hill, M.G., Barton, J.K., 2003. Nat. Biotechnol. 21, 1192.
Emrani, A.S., et al., 2016. Food Chem. 190, 115–121.
Fu, Y., et al., 2017. Sens. Actuators B: Chem. 249, 691–699.
Gerry, N.P., Witowski, N.E., Day, J., Hammer, R.P., Barany, G., Barany, F., 1999. J. Mol. Biol. 292, 251–262.
Green, N.S., Norton, M.L., 2015. Anal. Chim. Acta 853, 127–142.
Greiner, A., Joachim, H.W., 2007. Angew. Chem. Int. Ed. 46, 5670–5703.
Gumpu, M.B., Sethuraman, S., Krishnan, U.M., Rayappan, J.B.B., 2015. Sens. Actuators B: Chem. 213, 515–533.
Hahm, J.I., Lieber, C.M., 2004. Nano Lett. 4, 51–54.
Huang, H., Bai, W., Dong, C., Guo, R., Liu, Z., 2015. Biosens. Bioelectron. 68, 442–446.
Kallioniemi, A., et al., 1994. Proc. Natl. Acad. Sci. USA 91, 2156–2160.
Kim, D.S., et al., 2004. Biosens. Bioelectron. 20, 69–74.
Kim, K.H., et al., 2016. Sci. Rep. 6, 37783.
Kjallman, Tanja H.M., Peng, H., Soeller, C., Travas-Sejdic, J., 2008. Anal. Chem. 80, 9460–9466.
Ma, C., Wang, W., Mulchandani, A., Shi, C., 2014. Anal. Biochem. 457, 19–23.
Mahato, K., Maurya, P.K., Chandra, P., 2018. 3 Biotech 8, 149.
Matta, D.P., Tripathy, S., Vanjari, S.R.K., Sharma, C.S., Singh, S.G., 2016. Biomed. Micro. 18, 111.
Mistry, H., et al., 2016. PLoS One 11, e0162256.
Mukhopadhyay, R., Lorentzen, M., Kjems, J., Besenbacher, F., 2005. Langmuir 21, 8400–8408.
Naraghi, M., Arshad, S.N., Chasiotis, I., 2011. Polymer 52, 1612–1618.
Peng, H., Zhang, L., Soeller, C., Travas-Sejdic, J., 2009. Biomaterials 30, 2132–2148.
Prado, M., Ortea, I., Vial, S., Rivas, J., Calo-Mata, P., Barros-Velázquez, J., 2016. Crit. Rev. Food Sci. Nutr. 56, 2511–2542.
Schöler, A., Jacquiod, S., Vestergaard, G., Schulz, S., Schloter, M., 2017. Biol. Fertil. Soils 53, 485–489.
Sharon, E., Freeman, R., Willner, I., 2010. Anal. Chem. 82, 7073–7077.
Song, E., Choi, J.W., 2013. Nanomaterials 3 (3), 498–523.
Stafiniak, A., et al., 2011. Sens. Actuators B: Chem. 160, 1413–1418.
Thiha, A., et al., 2018. Biosens. Bioelectron. 107, 145–152.
Thomer, L., Schneewind, O., Missiakas, D., 2016. Annu Rev. Pathol. 11, 343–364.
Thompson, C.J., Chase, G.G., Yarin, A.L., Reneker, D.H., 2007. Polymer 48, 6913–6922.
Tripathy, S., Vanjari, S.R.K., Singh, V., Swaminathan, S., Singh, S.G., 2017a. Biosens. Bioelectron. 90, 378–387.
Tripathy, S., Naithani, A., Vanjari, S.R.K., Singh, S.G., 2017b. Proceedings of IEEE Sensors, pp. 1–3.
Tripathy, S., Ghole, A.R., Deep, K., Vanjari, S.R.K., Singh, S.G., 2017b. Food Chem. 217, 756–765.
Tripathy, S., Gangwar, R., Supraja, P., Rao, A.N., Vanjari, S.R.K., Singh, S.G., 2018. Electroanalysis 30, 2110–2120.
Wang, L., Li, P.C., 2011. Anal. Chim. Acta 687, 12–27.
Wang, X., Nan, F., Zhao, J., Yang, T., Ge, T., Jiao, K., 2015. Biosens. Bioelectron. 64, 386–391.
Yan, Y., Samai, S., Bischoff, K.L., Zhang, J., Ginger, D.S., 2016. ACS Sens. 1, 566–571.
Zhang, J.X., et al., 2018. Nat. Chem. 10, 91.
Zhang, Y., Rutledge, G.C., 2012. Macromolecules 45, 4238–4246.
Zheng, W., Lin, He, 2014. Biomater. Sci. 2, 1471–1479.